Journal of *Marine Science and Engineering*

MDPI

Article

A Joint Method on Dynamic States Estimation for Digital Twin of Floating Offshore Wind Turbines

Hao Xie [1], Ling Wan [1,*], Fan Shi [1], Jianjian Xin [1], Hu Zhou [2], Ben He [2], Chao Jin [3] and Constantine Michailides [4]

[1] Faculty of Maritime and Transportation, Ningbo University, Ningbo 315211, China; haoxie66888@163.com (H.X.); shifan@nbu.edu.cn (F.S.); xinjianjian@nbu.edu.cn (J.X.)
[2] Renewable Energy Engineering Division, Powerchina Huadong Engineering Corporation, Hangzhou 311122, China; zhou_h3@hdec.com (H.Z.); he_b2@hdec.com (B.H.)
[3] Zhejiang Zhoushan Offshore Wind Power Development Co., Ltd., Zhoushan, Guodian Power, Zhoushan 315042, China; jinc56806927@163.com
[4] Department of Civil Engineering, International Hellenic University, 57001 Thessaloniki, Greece; cmichailides@ihu.gr
* Correspondence: wanling@nbu.edu.cn

Abstract

Dynamic state estimation of floating offshore wind turbines (FOWTs) in complex marine environments is a core challenge for digital twin systems. This study proposes a joint estimation framework that integrates windowed dynamic mode decomposition (W-DMD) and an adaptive strong tracking Kalman filter (ASTKF). W-DMD extracts dominant modes under stochastic excitations through a sliding-window strategy and constructs an interpretable reduced-order state-space model. ASTKF is then employed to enhance estimation robustness against environmental uncertainties and noise. The framework is validated through numerical simulations under turbulent wind and wave conditions, demonstrating high estimation accuracy and strong robustness against sudden environmental disturbances. The results indicate that the proposed method provides a computationally efficient and interpretable tool for FOWT digital twins, laying the foundation for predictive maintenance and optimal control.

Keywords: FOWT; DMD; ROM; Kalman filter; estimation; digital twin

check for updates

Academic Editor: Rodolfo T. Gonçalves

Received: 1 September 2025
Revised: 26 September 2025
Accepted: 6 October 2025
Published: 16 October 2025

Citation: Xie, H.; Wan, L.; Shi, F.; Xin, J.; Zhou, H.; He, B.; Jin, C.; Michailides, C. A Joint Method on Dynamic States Estimation for Digital Twin of Floating Offshore Wind Turbines. *J. Mar. Sci. Eng.* **2025**, *13*, 1981. https://doi.org/10.3390/jmse13101981

Copyright: © 2025 by the authors. Licensee MDPI, Basel, Switzerland. This article is an open access article distributed under the terms and conditions of the Creative Commons Attribution (CC BY) license (https://creativecommons.org/licenses/by/4.0/).

1. Introduction

As the global energy structure accelerates the transformation to renewable energy, offshore wind power has become a key development direction of energy strategies in various countries due to its abundant resource reserves and high power generation efficiency. Since nearly half of the offshore wind resources are located in areas with water depth of 50 to 200 m, FOWT which is known to be suitable for water depth larger than 50 m, have significant development in recent years [1]. However, the FOWT system exhibits highly nonlinear dynamic characteristics in a complex marine environment (coupling of wind, waves, and currents), due to the strong coupling effects from aero-hydro-servo-elastic dynamic system [2]. These dynamic characteristics not only affect power generation efficiency but may also cause structural fatigue or even catastrophic failure. Accurate state estimation serves as the foundation for addressing these challenges. Without real-time monitoring and precise quantification of critical parameters, it becomes impossible to assess structural integrity, predict potential failures, or implement proactive control strategies. The harsh

marine environment introduces complex coupled dynamics between platform motions, turbine loads, and power generation systems, making state estimation particularly crucial for identifying abnormal operating conditions before they escalate, providing necessary feedback for advanced control algorithms, and enabling predictive maintenance through digital twin simulations. Therefore, high-precision state estimation (such as platform motion, tower load, generator speed, etc.) is a key link in the safe operation and performance optimization of floating wind power systems. It is also the core requirement for building a high-fidelity digital twin system [3].

Floating-body dynamics provides the fundamental framework for analyzing the motion and stability of offshore structures in ocean environments [4]. As a specific subset of this broader field, FOWTs pose additional challenges due to the strong coupling between aerodynamic loads, hydrodynamic forces, and structural flexibility. Currently, state estimation methods for FOWT are mainly divided into three categories: physical model-based methods, pure data-driven methods, and hybrid methods. Physical model-based approaches, such as the multibody dynamics simulation tool FAST/OpenFAST [5], rely on precise system parameters but are computationally expensive and prone to model errors when dealing with nonlinear and time-varying systems. In contrast, pure data-driven methods can directly learn system dynamics from operational data, offering an alternative to physics-based modeling.

However, data-driven techniques like LSTM [6] and GPR [7] have significant limitations. While LSTM excels at capturing temporal dependencies, its black-box nature makes it difficult to interpret results in terms of physical properties such as modal frequency, vibration shape, and damping ratio [8]. For example, Yin et al. [9] found that Bi-LSTM could predict platform responses accurately within 10 s but failed to explain the underlying physical relationships, restricting its use in control applications. Similarly, GPR provides probabilistic outputs with some interpretability, but its $O(n^3)$ computational complexity makes it impractical for real-time digital twin implementations [10].

In recent years, hybrid methods have emerged as a promising approach for FOWT state estimation by effectively combining physical mechanisms with data-driven advantages. Among these, DMD has gained significant attention due to its unique combination of physical interpretability, computational efficiency, and dimensionality reduction capabilities. Unlike purely data-driven black-box models, DMD extracts modes that directly correspond to system characteristic frequencies and vibration modes [11], enabling clear associations with actual physical phenomena such as platform oscillations and wave frequency resonance. The method's linear state-space architecture maintains relatively low computational complexity ($O(n^2)$) [12], making it suitable for real-time applications. Additionally, DMD's ability to extract dominant dynamic modes from high-dimensional sensor data significantly reduces the complexity of subsequent processing, addressing some of the key limitations of both purely physical and purely data-driven approaches. These characteristics position DMD as a particularly attractive solution for FOWT state estimation, bridging the gap between physical understanding and computational practicality in operational environments.

However, standard DMD is sensitive to noise and has difficulty processing non-stationary signals [13], and the strong nonlinearity of FOWT and environmental noise (such as high-frequency components of wave impact) further exacerbate this challenge. To enhance robustness, numerous advancements of the Kalman Filter (KF) have been developed over the past decades. The Extended Kalman Filter (EKF) remains one of the most widely used variants, in which system nonlinearities are handled through local linearization, although its accuracy may be degraded by approximation errors. To overcome this limitation, the Unscented Kalman Filter (UKF) applies an unscented transformation to

capture higher-order statistics without explicit linearization [14]. The Strong Tracking Filter (STF) adapts the filter gain in real time to track fast-changing dynamics [15]. In addition, Adaptive Kalman Filters (AKF) improve estimation under time-varying or uncertain noise by updating the noise covariance online, while the Ensemble Kalman Filter (EnKF) is particularly effective for large-scale, high-dimensional systems such as ocean circulation and weather prediction. Moreover, Robust Kalman Filters (RKF) have been designed to mitigate the impact of model uncertainties and outliers, and Particle Filters (PF)—though not strictly Kalman-based—are often employed as benchmarks for handling strongly nonlinear and non-Gaussian environments.

Recent studies highlight that KF and its variants are highly complementary to Dynamic Mode Decomposition (DMD). While DMD extracts low-dimensional, interpretable dynamic models, KF provides online correction and noise suppression to improve prediction accuracy. For instance, Kaneko et al. [16] integrated KF with DMD to significantly enhance the estimation efficiency of supersonic jet states, while Chen et al. [17] used KF as a preprocessing step in ship maneuvering signals and subsequently combined it with DMD to achieve high-precision prediction under real measurement conditions. This joint framework suggests promising potential for addressing the strong nonlinearity and environmental noise encountered in floating offshore wind turbine (FOWT) systems and other complex engineering applications.

To address the above problems, this paper proposes a W-DMD-ASTKF joint estimation method for FOWT digital twins. The main contributions include constructing a reduced-order model of the FOWT using the improved W-DMD algorithm, which effectively extracts dominant modes and dynamically updates the state equation for mode extraction, thereby enabling accurate state estimation of FOWTs under turbulent and stochastic wind–wave environments.

The overall workflow of the proposed study is illustrated in Figure 1. The framework follows a three-stage vertical logic: Build–Validate–Deploy. First, a reduced-order model of the FOWT is constructed; second, the constructed model is evaluated and validated, particularly through predictive performance tests to assess its suitability as a prior model for Kalman filtering; finally, the validated model is deployed in the joint estimation framework. In parallel, the horizontal logic extends from regular steady-wind conditions to stochastic wind–wave environments, ensuring the method's adaptability under increasingly realistic scenarios. The left-hand side of the schematic emphasizes model construction and evaluation, while the right-hand side highlights the deployment and application of the Kalman filter. This layered structure clearly demonstrates the progressive workflow of the proposed W-DMD-ASTKF framework.

Compared with prior studies, this work develops a W-DMD-ASTKF framework for FOWT digital twins. The proposed W-DMD updates the reduced-order model in sliding windows, enabling dynamic tracking of dominant modes under turbulent wind–wave excitations. By integrating the adaptive strong tracking Kalman filter, the method achieves robust state estimation even in the presence of modeling errors and environmental disturbances. This joint strategy bridges the gap between interpretability and real-time applicability: DMD provides physically meaningful modal representation, while ASTKF ensures accurate and adaptive estimation. This paper is organized as follows: Section 2 introduces the theoretical basis of DMD and KF; Section 3 introduces the source of training data and simulation methods; Section 4 results and discussions; Section 5 conclusions.

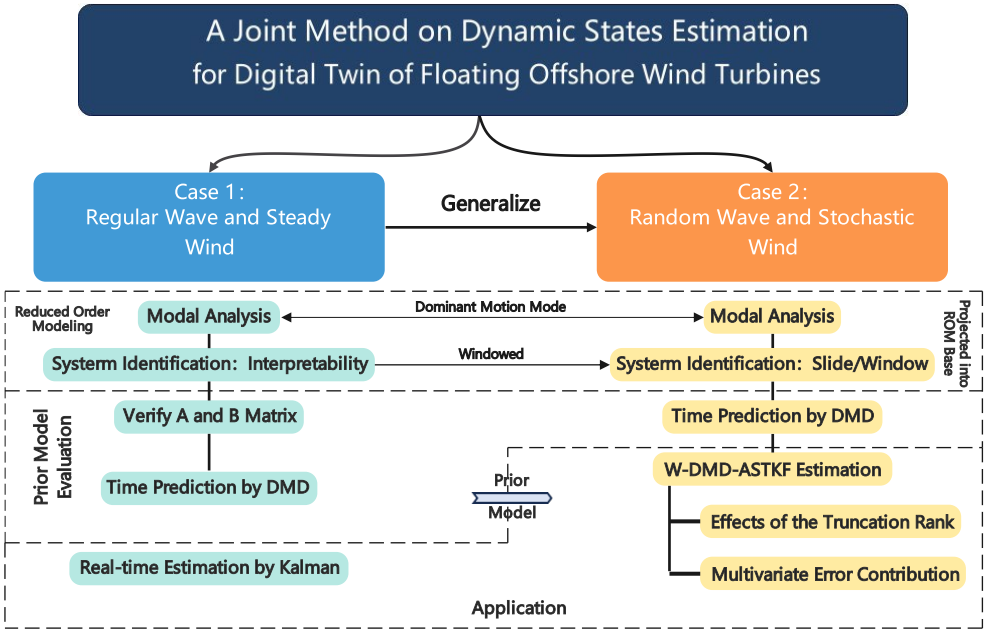


Figure 1. Schematic diagram of our work.

2. Methodology

This section introduces the proposed method for real-time state estimation and prediction of FOWT under random environmental loads. The method combines DMD for system dynamics extraction and KF [18] for state estimation and noise suppression. The DMD module uses the Python open source tool PyDMD (Version 2025.4.1) [19] to achieve efficient modal calculation and KF for state estimation and noise suppression.

2.1. Dynamic Mode Decomposition (DMD) Theory

DMD is a data-driven method for extracting dominant spatio-temporal modes from high-dimensional dynamic system data. This method is essentially a modal decomposition technique based on the Koopman operator [20]. The Koopman operator provides a theoretical framework for DMD by mapping nonlinear dynamic systems into infinite-dimensional linear space [21]. For the complex dynamic system of floating offshore wind turbines, we use an improved DMD algorithm (including adaptive window selection and noise robustness processing) to establish its reduced-order model (see Figure 2). It should be noted that, as a fundamentally linear technique, DMD may not fully capture all nonlinear dynamics inherent in floating offshore wind turbines, and the results should be interpreted within this approximation.

2.1.1. Implementation of DMD Algorithm for Reduced-Order Reconstruction Prediction

Assemble a high-dimensional time series data matrix consisting of wind turbine system state variables [22] $\mathbf{X}$ and $\mathbf{X}'$:

$$\mathbf{X} = \begin{bmatrix} | & | & & | \\ \mathbf{x}(t_1) & \mathbf{x}(t_2) & \cdots & \mathbf{x}(t_{n-1}) \\ | & | & & | \end{bmatrix} \in \mathbb{R}^{m\times(n-1)}$$

$$\mathbf{X}' = \begin{bmatrix} | & | & & | \\ \mathbf{x}(t_2) & \mathbf{x}(t_3) & \cdots & \mathbf{x}(t_n) \\ | & | & & | \end{bmatrix} \in \mathbb{R}^{m\times(n-1)}$$

where $\mathbf{X}'$ is the state of $\mathbf{X}$ at the next moment, that is:

$$\mathbf{X}' \approx \mathbf{A}\mathbf{X} \tag{1}$$

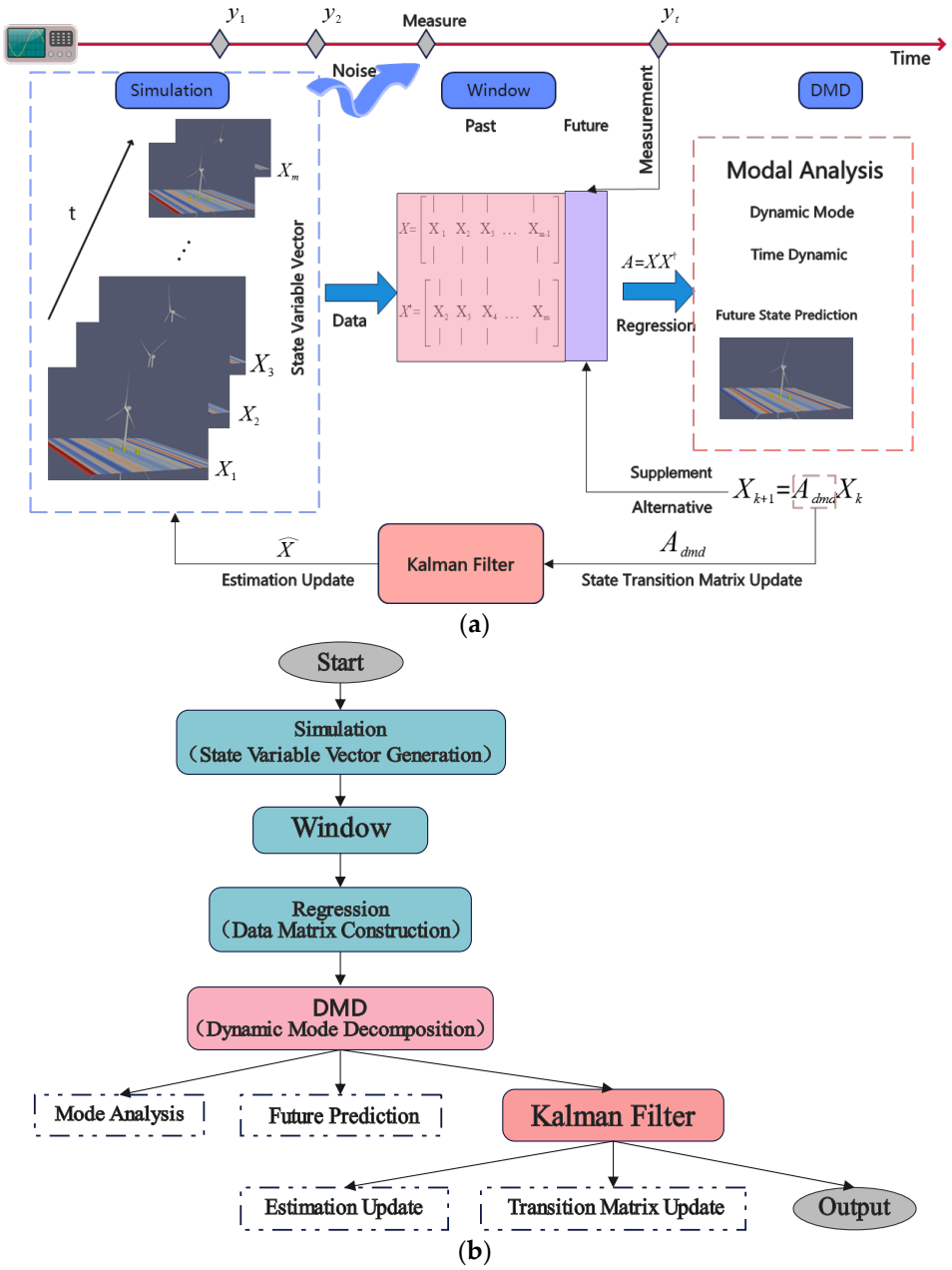


Figure 2. (**a**) Schematic of the W-DMD-ASTKF Framework, where † denotes the Moore–Penrose pseudoinverse; (**b**) Flowchart of the W-DMD-ASTKF.

In this study, **A** is the state transfer matrix describing the discrete-time linear dynamics of the offshore platform motion, capturing the dynamic characteristics of the offshore platform motion (such as vibration modes under wave and wind excitation). The state matrix **X** includes 16 key state variables, which fully describe the system dynamics behavior:

1. Six D.O.F floating body motions [23] (displacement): Translation: surge, sway, heave; Rotation: roll, pitch, yaw (variable selection refers to the full-scale prototype study of floating wind power [24]);
2. Tower and wind turbine dynamic variables: fore-aft displacement, rotational speed;

3. First-order time derivatives of all the above variables (used to construct state-space equations, see DMD system identification study in FOWT) [25].

Through SVD and low-rank reconstruction, we obtain a low-dimensional approximate matrix $\widetilde{\mathbf{A}}$, which is the optimal low-rank representation of $\mathbf{A}$ in the modal space, approximating the dominant mode of the original dynamics $\mathbf{A}$, and can be used to predict the vibration response of marine platforms or identify key frequencies. The specific steps are as follows:

Step1: SVD

Perform SVD on $\mathbf{X}$:

$$\mathbf{X} = \mathbf{U}_r \mathbf{\Sigma}_r \mathbf{V}_r^* \tag{2}$$

where $\mathbf{U}_r \in \mathbb{C}^{n\times r}$, $\mathbf{\Sigma}_r \in \mathbb{C}^{r\times r}$, $\mathbf{V}_r \in \mathbb{C}^{m\times r}$, r is the truncated rank (reduced dimensionality), is determined by retaining 95% of the total singular value energy.

Step2: Low Dimensional Mapping

Project the high-dimensional $\mathbf{A}$ into the low-dimensional space (the space spanned by $\mathbf{U}_r$)

$$\widetilde{\mathbf{A}} = \mathbf{U}_r^* \mathbf{A} \mathbf{U}_r = \mathbf{U}_r^* \mathbf{X}' \mathbf{V}_r \mathbf{\Sigma}_r^{-1} \tag{3}$$

Here is a reduced-order representation of $\widetilde{\mathbf{A}} \in \mathbb{C}^{r\times r}$ that captures the dominant dynamic modes.

Step3: Eigenvalue and Eigenvector

$$\widetilde{\mathbf{A}}\mathbf{W} = \mathbf{W}\mathbf{\Lambda} \tag{4}$$

where the eigenvalue $\mathbf{\Lambda}$ represents the growth/decay rate of the dynamic mode, and the eigenvector $\mathbf{W}$ columns correspond to the dynamic modes.

Step4: DMD Mode

$$\mathbf{\Phi} = \mathbf{X}' \mathbf{V}_r \mathbf{\Sigma}_r^{-1} \mathbf{W} \tag{5}$$

$$\mathbf{f}_i = \frac{\mathrm{Im}(\ln(\lambda_i))}{2\pi \Delta \mathbf{t}} \tag{6}$$

$$\zeta_i = -\frac{\mathrm{Re}(\ln(\lambda_i))}{2\pi f_i \Delta \mathbf{t}} \tag{7}$$

where the column vector of $\mathbf{\Phi}$ is the dynamic mode in space, λ_i is the i-th eigenvalue of DMD, $\Delta \mathbf{t}$ represents the sampling time interval and ζ_i is the damping ratio.

Step5: Prediction

$$\mathbf{x}_k \approx \sum_{i=1}^{r} \mathbf{b}_i \boldsymbol{\phi}_i \lambda_i^{k-1} \tag{8}$$

where $\mathbf{b} = \mathbf{\Phi}^{\dagger} \mathbf{x}_1$ (projection of the initial value onto the vector); $\mathbf{\Phi}^{\dagger}$ is the Moore- Penrose pseudoinverse of $\mathbf{\Phi}$; λ is the eigenvalue; $|\lambda_i|$ the amplitude of the eigenvalue indicates the stability of the corresponding mode.

This process enables us to capture the dominant dynamic characteristics of floating wind turbines under random environmental excitations such as waves and wind loads [26].

2.1.2. Delay Embedding and Hankel Matrix Construction

For a given state variable time series:

$$\mathbf{x}_1, \mathbf{x}_2, \mathbf{x}_3, \cdots, \mathbf{x}_m$$

$$\mathbf{H}_d = \begin{bmatrix} \mathbf{x_1} & \mathbf{x_2} & \mathbf{x_3} & \cdots & \mathbf{x_{m-\tau}} \\ \mathbf{x_2} & \mathbf{x_3} & \mathbf{x_4} & \cdots & \mathbf{x_{m-\tau+1}} \\ \vdots & \vdots & \vdots & \ddots & \vdots \\ \mathbf{x_\tau} & \mathbf{x_{\tau+1}} & \mathbf{x_{\tau+2}} & \cdots & \mathbf{x_m} \end{bmatrix}$$

Finding $\mathbf{A}_d$ to establish the state transfer relationship between $\mathbf{H}_d$ and $\mathbf{H'}_d$ can better capture the nonlinear dynamic relationship, but it will introduce false modes.

2.1.3. Time-Varying DMD Expansion

To deal with the nonlinear characteristics of floating wind turbines under time-varying environmental loads, we use a sliding window DMD method:

1. Define the sliding window length L and step size $\boldsymbol{\Delta t}$
2. Perform DMD analysis on each window data;
3. Establishing a time-varying state transfer matrix sequence.

This method can adaptively track changes in the system's dynamic characteristics and improve long-term prediction accuracy [27].

2.2. System Identification Theory

Based on the reduced-order model extracted from DMD, we further establish the state space representation of the floating wind turbine.

2.2.1. State Space Modeling

$$\mathbf{x}_{k+1} = \mathbf{A}\mathbf{x}_k + \mathbf{B}\mathbf{u}_k + \mathbf{w}_k \tag{9}$$

$$\mathbf{y}_k = \mathbf{H}\mathbf{x}_k + \mathbf{D}\mathbf{u}_k + \mathbf{v}_k \tag{10}$$

where $\mathbf{A} \in \mathbb{R}^{r\times r}$ is the state transition matrix derived from DMD, $\mathbf{B} \in \mathbb{R}^{r\times p}$ is the control input matrix (p is the dimension of the control variable, $\mathbf{H} \in \mathbb{R}^{q\times r}$ is the observation matrix (q is the dimension of the observation variable), $\mathbf{D} \in \mathbb{R}^{q\times p}$ is the Direct transfer matrix, $\mathbf{w}_k \sim \mathcal{N}(\mathbf{0}, Q)$ is the process noise, $\mathbf{v}_k \sim \mathcal{N}(\mathbf{0}, R)$ is the measurement noise.

Different from the traditional physical model-based method, this method obtains $\mathbf{A}$ in a data-driven way, which is particularly suitable for complex coupled systems such as floating wind turbines that are difficult to model accurately [28].

2.2.2. Model Parameter Identification

Using the least squares method to estimate:

$$\min_{\mathbf{A},\mathbf{B}} J(\mathbf{A},\mathbf{B}) = \sum_{k=1}^{N-1} \left|\left| \epsilon_k \right|\right|_2^2 = || \mathbf{X'} - \mathbf{A}\mathbf{X} - \mathbf{B}\mathbf{U} ||_F^2 \tag{11}$$

Dynamic modal modeling B is established by using an augmented matrix with external input:

$$\mathbf{\Omega} = \begin{bmatrix} \mathbf{X} \\ \mathbf{U} \end{bmatrix}$$

Perform DMD on the augmented matrix to obtain system identification A and B.

State residual:

$$\mathbf{r}_k^{\mathbf{x}} = \mathbf{x}_{k+1} - \hat{\mathbf{x}}_{k+1} = \mathbf{x}_{k+1} - (\mathbf{A}\mathbf{x}_k + \mathbf{B}\mathbf{u}_k) \tag{12}$$

Observation residual:

$$\mathbf{r}_k^{\mathbf{y}} = \mathbf{y}_k - \hat{\mathbf{y}}_k = \mathbf{y}_k - (\mathbf{C}\hat{\mathbf{x}}_k + \mathbf{D}\mathbf{u}_k) \tag{13}$$

2.3. Data Assimilation and Kalman Filter

The DMD model is combined with the Kalman filter (see Figure 3) to form a real-time state estimation framework. The algorithm is divided into two stages:

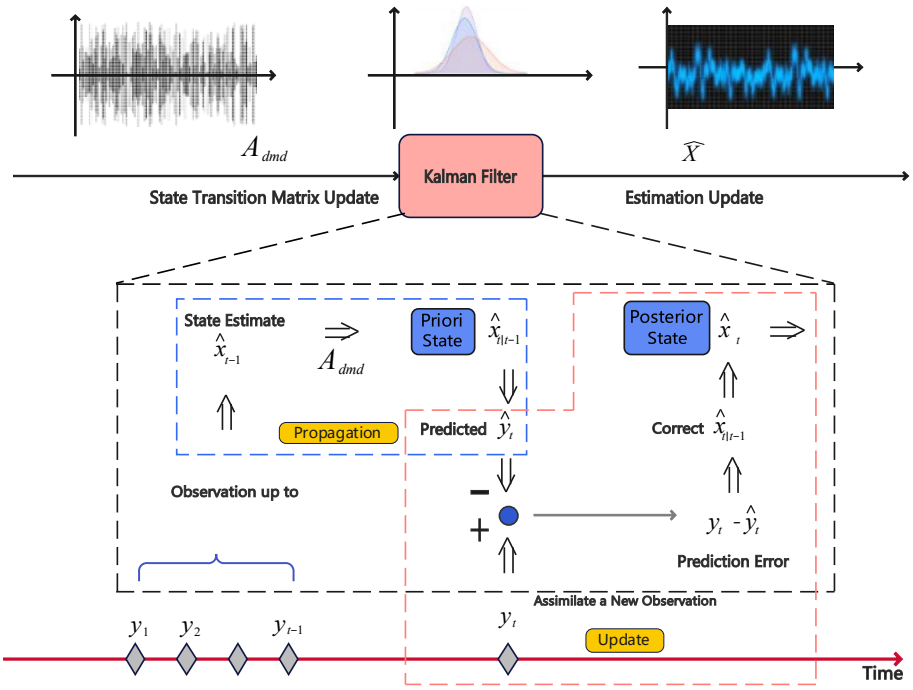


Figure 3. Internal Architecture of the ASTKF.

2.3.1. Standard Kalman Filter Implementation

Prediction:

$$\hat{\mathbf{x}}_k^- = \mathbf{A}\hat{\mathbf{x}}_{k-1} + \mathbf{B}\mathbf{u}_{k-1} \tag{14}$$

$$\mathbf{P}_k^- = \mathbf{A}\mathbf{P}_{k-1}\mathbf{A}^T + \mathbf{Q} \tag{15}$$

where $\hat{\mathbf{x}}_k^-$ the prior state estimation, the $\mathbf{P}_k^-$ prior state estimation error covariance matrix.

Data fusion and update:

$$\mathbf{K}_f = \mathbf{P}_k^-\mathbf{H}^T(\mathbf{H}\mathbf{P}_k^-\mathbf{H}^T + \mathbf{R})^{-1} \tag{16}$$

$$\hat{\mathbf{x}}_k = \hat{\mathbf{x}}_k^- + \mathbf{K}_f\left(\mathbf{y}_k - \mathbf{H}\hat{\mathbf{x}}_k^- - \mathbf{D}\mathbf{u}_k\right) \tag{17}$$

$$\mathbf{P}_k = (\mathbf{I} - \mathbf{K}_k\mathbf{H})\mathbf{P}_k^- \tag{18}$$

where $\mathbf{K}_f$ the Kalman gain that was used to fuse measurement data and model prediction data, $\hat{\mathbf{x}}_k$ the posterior state estimation, $\mathbf{P}_k$ the posterior state estimation error covariance matrix.

2.3.2. Improvement Measures for Floating Offshore Wind Turbines

Adaptive Noise Covariance:

$$\tilde{\mathbf{Q}}_k = (1-\alpha)\tilde{\mathbf{Q}}_{k-1} + \alpha\left(\mathbf{K}_k\mathbf{v}_k\mathbf{v}_k^T\mathbf{K}_k^T + \mathbf{P}_k - \mathbf{A}\mathbf{P}_{k-1}\mathbf{A}^T\right) \tag{19}$$

where α is forgetting factor; in calm sea conditions, a smaller α is used to maintain the stability of the DMD prior; in rough sea/gust conditions, a slightly larger α is adopted to quickly correct Q. The initial screening range of α is set to [0.02, 0.1].

In realistic offshore conditions, the motions of floating wind turbines are influenced by time-varying wind, wave, and current loads, which make the noise statistics non-stationary. To address this, the Sage–Husa adaptive algorithm [29] is applied to update the process and measurement noise covariance matrices online. The algorithm dynamically adjusts these parameters through MAP estimation using real-time measurements of the platform's six degrees of freedom (surge, sway, heave, roll, pitch, yaw), tower-top displacements, and rotor speed. This enables the filter to capture changes in noise characteristics under gradually varying operating conditions, such as linearly increasing or decreasing environmental loads, and ensures accurate motion DOF estimation across different sea states.

In this study, the update threshold is determined based on statistical analysis of the forecast error, which is quantified using the RMSE between the predicted and measured motion responses (platform degrees of freedom, tower-top displacement, and rotor speed). Historical datasets under representative environmental and operational conditions are analyzed to obtain the statistical distribution of the RMSE. The threshold is then defined as the mean value plus three standard deviations, corresponding to a 99.7% confidence interval under the Gaussian assumption. This choice ensures that updates are triggered only when prediction accuracy significantly deteriorates, while avoiding unnecessary recomputation under normal operating conditions. Although the present work adopts this statistical criterion, the framework is general: in future applications, the threshold may be further tuned through sensitivity analysis or adjusted according to specific monitoring objectives.

3. Model Descriptions and Numerical Simulation Setup

This chapter details the numerical simulation setup of the IEA-15MW FOWT. The IEA-15MW is a benchmark model defined by the IEA Wind TCP. Its design parameters are detailed in the technical report [30]. The research focuses on the semi-submersible floating platform VolturnUS-S developed by the University of Maine (UMaine) in the United States. The technical specifications of the platform can be found in the design documents publicly available from UMaine [31]. The numerical simulation uses the OpenFAST v3.0 multi-body dynamics simulation tool [32] and TurbSim v2.0 turbulence field generation software [33] developed by the National Renewable Energy Laboratory (NREL) of the United States. The experiment strictly follows the modeling specifications of the OpenFAST User Manual (NREL, 2022a) [32] and generates a turbulent wind field that meets the IEC standard based on the TurbSim Technical Manual (NREL, 2022b) [33]. High-precision numerical simulation is carried out under two types of environmental conditions to obtain dynamic response data of floating wind turbines, providing data support for the subsequent verification of DMD.

3.1. FOWT Model and Numerical Simulation Setup

This study uses the IEA-15MW reference wind turbine as the research object. The unit is installed on the VolturnUS-S semi-submersible floating platform developed by the University of Maine (UMaine) in the United States (see Figure 4). The platform adopts a three-column semi-submersible structure design. By optimizing the waterline area and ballast distribution, it effectively reduces the motion response while ensuring stability. The platform has a main body diameter of 40 m and a draft of 20 m. It is positioned using a catenary mooring system and is suitable for deep sea areas with a water depth greater than

100 m. The supporting wind turbine has a rated power of 15 MW, a rotor diameter of 240 m, and a hub height of 150 m.

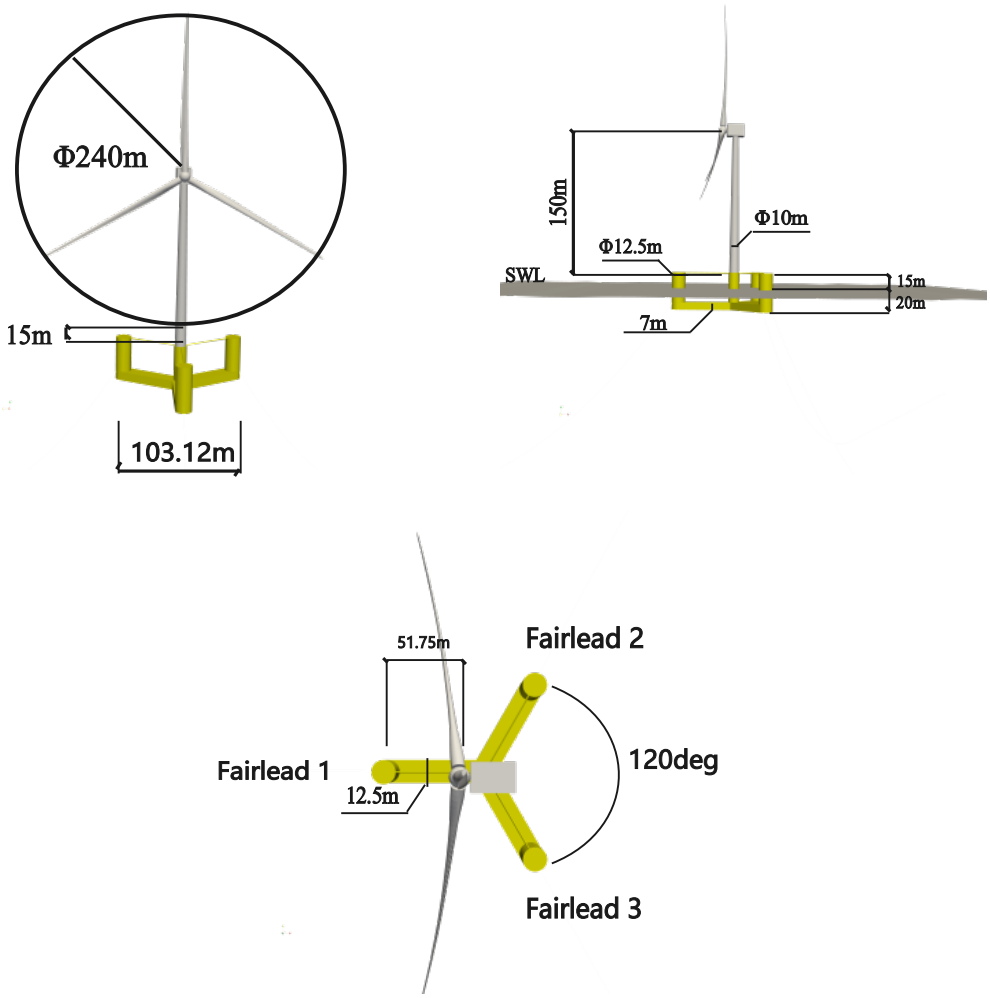


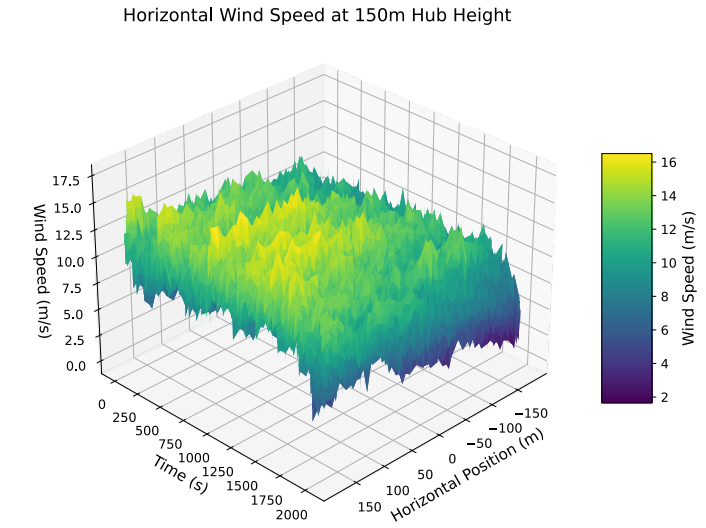
Figure 4. IEA 15-MW Reference Turbine and VolturnUS-S Semi-submersible (adapted from the one provided by the University of Maine [30]).

The numerical model is built on the OpenFAST open-source platform developed by the National Renewable Energy Laboratory (NREL) of the United States. The hydrodynamic characteristics of the floating platform were specially processed during the modeling process: The frequency domain hydrodynamic coefficients of the platform were calculated using the WAMIT software; The mooring system model was established using the MoorDyn module to accurately consider the geometric nonlinear effects of the catenary. The wind field simulation uses TurbSim to generate a turbulent field that complies with the International Electrotechnical Commission (IEC) 61400-1 Ed.4 standard [34], and its parameter settings meet the requirements of DNV-ST-0119 "Floating Wind Turbines" for dynamic analysis of offshore floating wind turbines [35]. Based on the Kaimal turbulence spectrum model, the cut-in to cut-out wind speed range is covered. The wave field uses the JONSWAP spectrum to simulate irregular waves to reflect the characteristics of actual sea conditions. The specific simulation parameters are set as follows: 0° wave direction angle, 0° horizontal wind direction angle, 2 m/s ocean current velocity, and a 0.12 power exponential wind speed distribution along the height direction (Figure 5b).

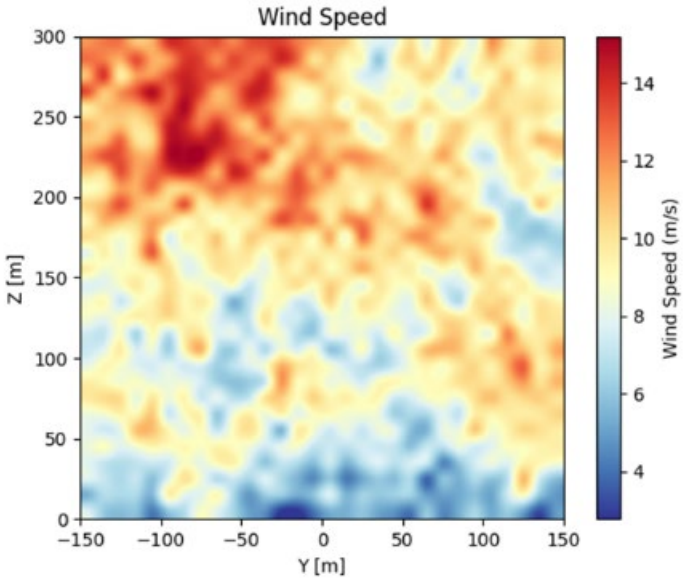
The experiment calculates 10 related state variables and applies Gaussian noise to these variables to simulate 10 sensors with a sampling frequency of 40 Hz (6 platform motion sensors, 1 tower top displacement sensor, 1 anemometer (at hub height), 2 probes),

which are used to monitor the Heave, Surge, Pitch, Roll, Yaw, Sway motion response of the floating wind power system, as well as state variables such as tower top displacement and wind turbine speed, while recording the input variables wave height and wind speed. The study designed 8 working conditions (DLC):

1. DLC1: Regular wave steady wind condition;
2. DLC7: Steady wind random wave conditions;
3. DLC2-6 & DLC8: Irregular wave turbulent wind conditions.



(**a**)



(**b**)

Figure 5. Wind Field Inputs for Numerical Simulations: (**a**) Turbulent Wind Speed (Uw) Time Series at Hub Height (DLC2, 0–1800 s); (**b**) Vertical Distribution of Mean Wind Speed.

Among them, DLC2 uses a significant wave height of 1.54 m and a spectral peak period of 7.65 s. The measured Surge is shown in Table 1. DLC5-6 is specifically used to verify the effect of DMD under non-stationary wind speed changes. Based on the assumption of 3 h stability of the wave environment, the simulation time of each condition is 1800 s, and 4 sets of repeated samples are set. Finally, 32 time series datasets are obtained (Table 1),

which contain a total of 256 state variables for verifying the accuracy of the joint DMD and Kalman recursive reduction algorithm.

Table 1. Environmental Condition Inputs: Sampling Intervals and Data Ranges.

Case	DLC	TS	Hs (m)	Tp (s)	SI (s)	Vel_Mean (m/s)	Vel_Std (m/s)	Ele_Mean (m)	Ele_Std (m)
C1	DLC1	S1 S2 S3 S4	5 m	10 s	A B C D	10	0	−0.0009	1.764
C2	DLC2	S5	5 m	10 s	A	9.51	0.56	−0.0203	1.0613
		S6			B	7.86	0.49	0.12	1.34
		S7			C	9.39	0.95	−0.013	1.5
		S8			D	10.41	0.69	0.067	0.835
	DLC3	S9	1.54 m	7.65 s	A	10.42	0.55	−0.0037	0.3196
		S10			B	10.006	0.86	0.016	0.375
		S11			C	10.205	0.866	0.0059	0.439
		S12			D	11.93	0.952	0.015	0.32
	DLC4	S13	3 m	6 s	A	10.42	0.56	−0.012	0.75
		S14			B	10.006	0.869	0.002	0.576
		S15			C	10.205	0.866	0.0058	0.776
		S16			D	11.93	0.952	0.011	0.53
	DLC5	S17	3 m	6 s	A	6.29	0.05	−0.012	0.75
		S18			B	6.78	0.05	0.002	0.576
		S19			C	7.26	0.05	0.005	0.776
		S20			D	7.75	0.05	0.011	0.532
	DLC6	S21	3 m	6 s	A	9.49	0.028	−0.012	0.75
		S22			B	9.25	0.028	0.002	0.576
		S23			C	9	0.028	0.005	0.776
		S24			D	8.76	0.028	0.011	0.53
	DLC7	S25	3 m	6 s	A	10	0	−0.01	0.75
		S26			B			0.054	1.06
		S27			C			0.0105	1.29
		S28			D			0.05	0.887
	DLC8	S29	7 m	10 s	A	10.42	0.55	−0.006	1.694
		S30			B	10.006	0.869	0.153	1.73
		S31			C	10.205	0.866	−0.011	2.104
		S32			D	11.931	0.952	0.078	0.977

Note: DLC stands for design load condition, TS stands for Time_Sample, Vel_Mean stands for horizontal wind speed mean,Vel_Std stands for horizontal wind speed standard deviation, Ele_Mean stands for Wave Elevation Mean, Ele_Std stands for Wave Elevation standard deviation. A stands for 1685 s–1725 s, B stands for 1585 s–1625 s, C stands for 1492 s–1532 s, D stands for 1385 s–1425 s.

3.2. Data Preprocessing and Performance Evaluation Indicators

The first-order terms are calculated by performing time difference calculation on the state variables, and the characteristic quantities such as the mean, standard deviation and extreme value of the statistical analysis response are calculated (see Table 1, Figure 6). The overall statistical analysis of the 8-DOF system response during the full simulation period (0–1800 s) is summarized in Table 2. The platform heave response frequency is identified using Dynamic Mode Decomposition, as shown in Figure 7. The FFT of the DLC2 time series is then analyzed to extract the main steady-state response frequencies (Figure 8).

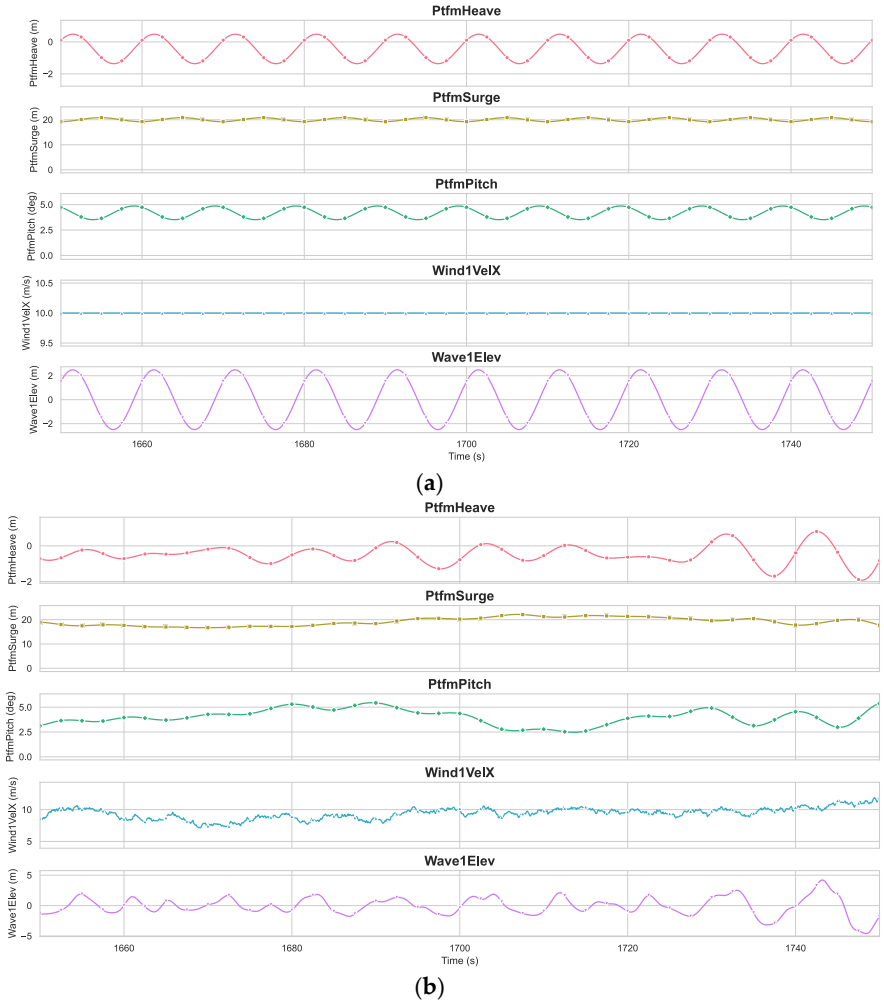


Figure 6. Dynamic Responses Under Different Environmental Conditions (1650–1750 s): (**a**) Heave, Surge, and Pitch in Steady Wind with Regular Waves (DLC1); (**b**) Heave, Surge, and Pitch in Turbulent Wind with Random Waves (DLC2).

Table 2. Statistical Analysis of 8-DOF System Response During Full Simulation Period (0–1800 s).

	Heave (m)	Surge (m)	Pitch (deg)	Sway (m)	Roll (deg)	Yaw (deg)	Rotspeed (m/s)	TTDspFA (m)
DLC1_Mean	0.4398	19.7061	4.1216	0.2379	0.3899	0.3158	6.9402	0.3304
DLC1_Std	0.6652	2.1798	0.5858	0.0452	0.0995	0.043	0.2288	0.077
DLC2_Mean	0.4405	18.8909	3.7191	0.2044	0.4042	0.6595	6.875	0.2927
DLC2_Std	0.4579	2.9385	0.8568	1.3918	0.1953	1.2448	0.6356	0.0984

The single state variable:

$$\mathrm{RMSE}_{\mathbf{x}} = \sqrt{\frac{\mathbf{1}}{N}\sum_{i=1}^{N}\left(\mathbf{x}_i^{\mathrm{true}} - \mathbf{x}_i^{\mathrm{est}}\right)^2} \tag{20}$$

Overall State Variables:

$$\mathrm{RMSE}_{\mathrm{Overall}} = \sqrt{\frac{\mathbf{1}}{mn}\sum_{j=1}^{m}\sum_{i=1}^{n}\left(\mathbf{x}_{i,j}^{\mathrm{true}} - \mathbf{x}_{i,j}^{\mathrm{est}}\right)^2} \tag{21}$$

4. Results and Discussions

4.1. Case 1: Regular Wave and Steady Wind

4.1.1. Dominant Mode Extraction and Frequency Domain Verification

In this study, the DMD method was used to analyze the time series data of the platform's heave motion in the 1600–1700 s time period. Formula (5) was directly applied to extract the dominant modal characteristics, avoiding false modal information from delayed embedded Hankel matrix construction and SVD truncation. The results show that the dominant oscillation mode frequency of the platform is 0.628 rad/s (Figure 7), consistent with the response frequency range predicted by classical linear wave theory. The real parts of all modal eigenvalues are negative ($\sigma < 0$), indicating that all eigenvalues are within the unit circle ($|\lambda| < 1$). The system is stable during the iterative evolution process without modal amplitude divergence.

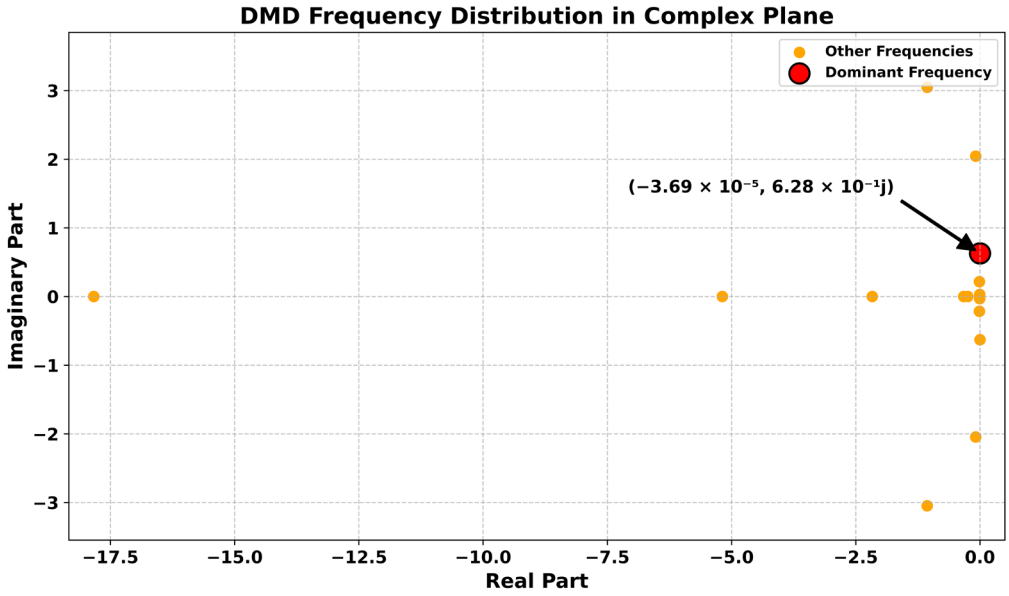


Figure 7. Platform Heave Response Frequency Identification via Dynamic Mode Decomposition.

FFT spectral analysis of the heave response also shows a significant peak at 0.63 rad/s (Figure 8), with a relative error of less than 0.3% compared with DMD. This confirms the accuracy of DMD modal identification and shows that the heave response can be approximated as a linear time-invariant system. DMD directly evaluates system stability through eigenvalue real parts and simultaneously provides modal frequency and growth rate information, making it more interpretable for dynamic mechanism analysis.

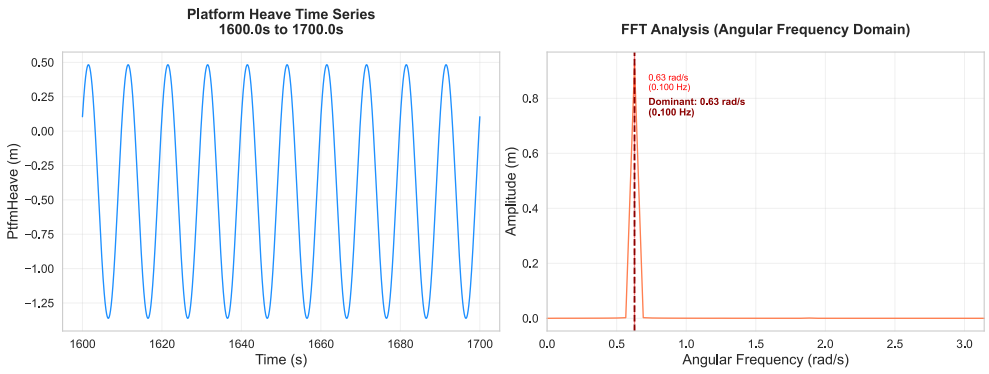


Figure 8. FFT Spectrum of PtfmHeave (1600–1700 s): Dominant Frequency Identification.

4.1.2. Reduced-Order Modeling and Physical Interpretation

Considering that the platform's motion under this operating condition exhibits weak nonlinearity, it can still be approximated as a linear time-invariant system. This study employed SVD (Equation (4)) to decompose the data matrix over the time period 1685–1700 s, calculating the singular values of each order and their relative energy contributions (see Figure 9). The results show that the cumulative energy contribution of the first six singular values exceeds 95%, with the first order alone contributing 69.8%, indicating that these six modes are the primary determinants of the system's dynamic characteristics. Based on the energy truncation criterion (a cumulative contribution $\geq$ 90% negates the influence of higher-order modes), this study ultimately adopted a 6-mode truncation.

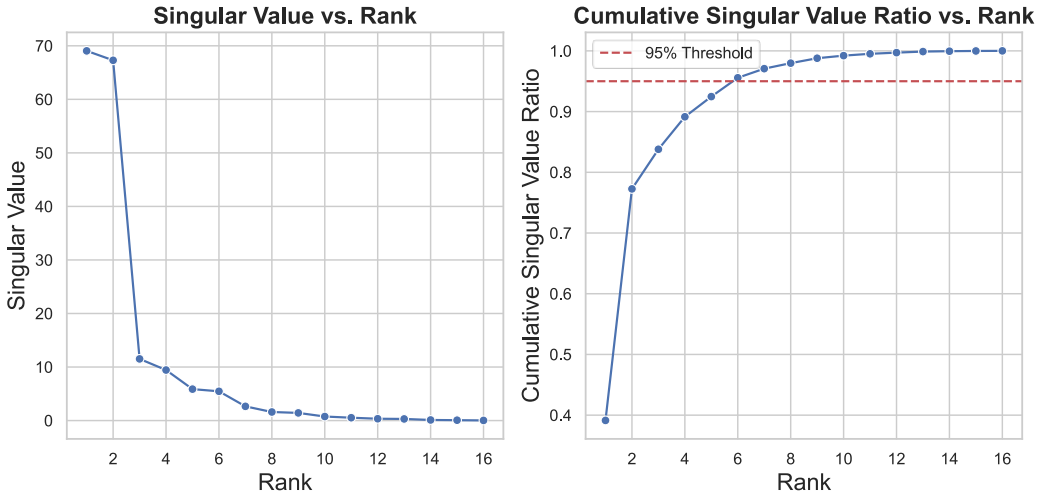


Figure 9. Determination of Model Order Reduction Threshold via Singular Value Analysis.

DMDc method is used to identify the data of the 1685–1700 s under the DLC1 condition, and the state transfer matrix $\mathbf{A} \in \mathbb{R}^{16\times16}$ and input matrix $\boldsymbol{B} \in \mathbb{R}^{16\times2}$ of the floating wind power system are obtained. Input variables include: input 1: wave elevation; input 2: wind speed. The state transfer matrix A describes the linear evolution relationship between the various state quantities within the system, while the input matrix B characterizes the impact of external excitations (waves and wind speed) on the system state, thereby jointly constructing a linearized dynamic model of the floating wind power system under this working condition.

Heatmap visualization of matrix A (Figure 10) shows all elements < 1, ensuring stability. A exhibits a symmetrical structure, reflecting bidirectional coupling of energy transfer. The 4th and 15th diagonal elements, corresponding to platform sway velocity and turbine speed, are dominant. Matrix B indicates that wave elevation strongly excites sway velocity, while wind speed input has limited effect on blade speed, likely due to controller regulation. Compared to black-box models like LSTM, DMDc provides a physically interpretable matrix structure that directly reveals the relationship between state coupling and input sensitivity.

4.1.3. Performance Evaluation and Filtering Optimization

Based on the rank-6 identification matrices A and B, combined with the 16-dimensional initial state at 1685 s and the input sequence from 1685 to 1700 s, the model was predicted (see Figure 11). The results show that the reduced-order model can well reproduce the normalized motion responses of the platform's heave, surge, and pitch. In particular, it is highly consistent with the measured data during the ascent and descent phases (average relative error < 9%), but deviations still exist at the turning points of the motion direction.

Comparison with measured data shows that the reduced-order model effectively preserves the core dynamic characteristics of the platform while reducing computational complexity, providing solid numerical support for the Kalman filter's state estimation.

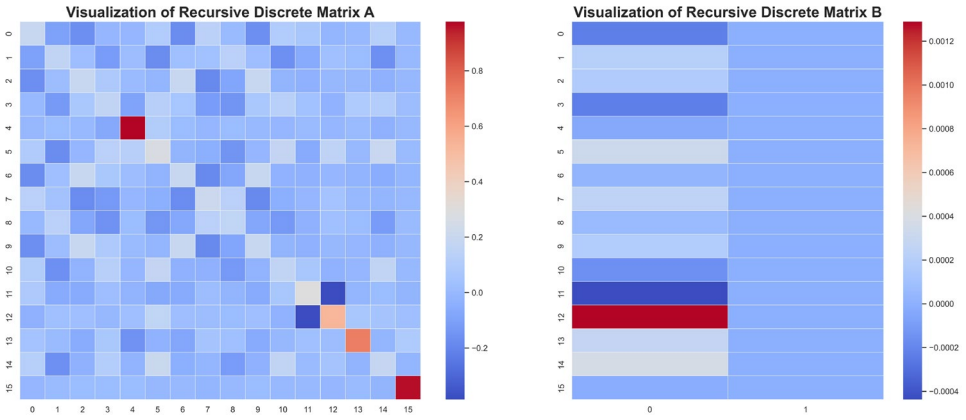


Figure 10. Heat Maps of Identified A (Dynamics) and B (Control) Matrices.

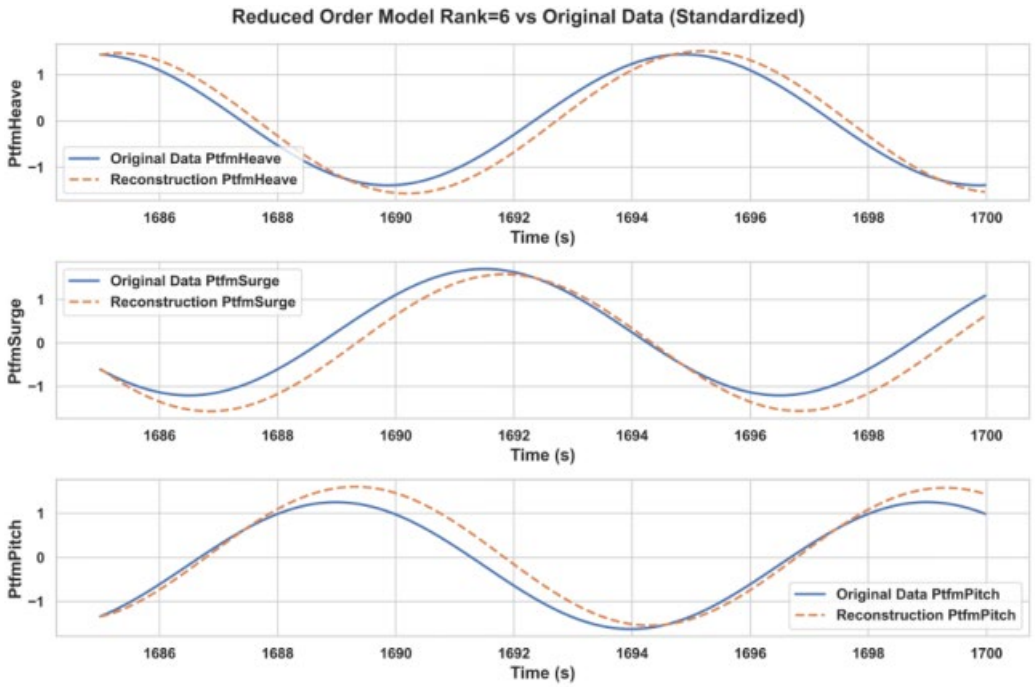


Figure 11. ROM-Predicted Platform Motions Using Constant A/B Matrices (Comparison of heave, surge, and pitch responses to environmental inputs during 1685–1700 s).

The model's short-term prediction capability was tested on the 1685–1725 s period of the S1 dataset. Samples 0–600 were used for training and 600–1600 for testing. The DMD predictions (green dashed line) closely matched measured values (orange solid line) (Figure 12). Heave motion prediction error was nearly zero in the test phase. Error accumulation appears in longer-term predictions, suggesting the need for online updating mechanisms in engineering applications.

To reduce turning point prediction bias, a Kalman filter was introduced. Assuming full observation of the 16-dimensional state (H = I), Gaussian white noise ($\sigma = 0.5$) was added to the output, and filtering recursion was performed (Equations (8) and (9)) (Figure 13). The filter estimates quickly converge to the true state and maintain accuracy at turning points, with maximum error < 0.15. Compared with direct observation, the Kalman filter

reduces turning point peak error by 73.2%, significantly improving responsiveness to sudden dynamic changes.

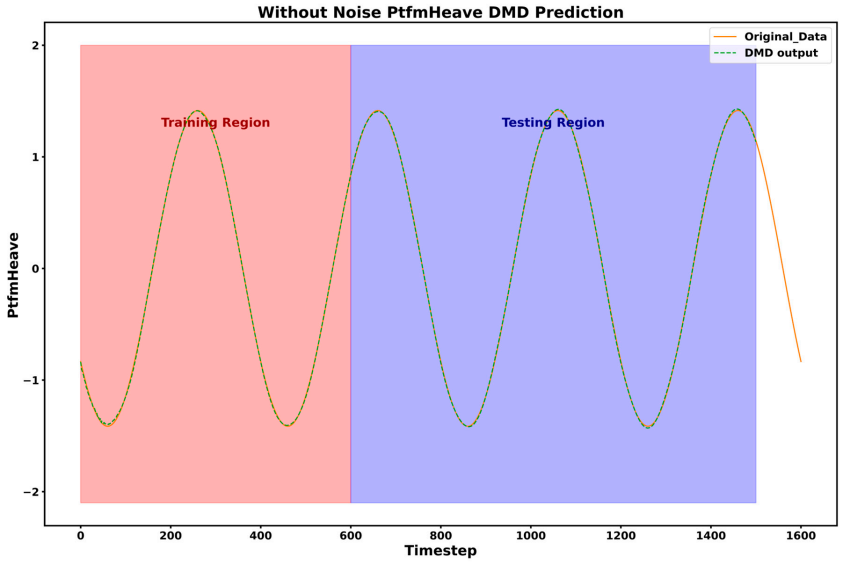


Figure 12. Sample 1:Heave Motion Prediction via DMD: Clean Training Phase (0–600) and Extended Prediction Phase (600–1500).

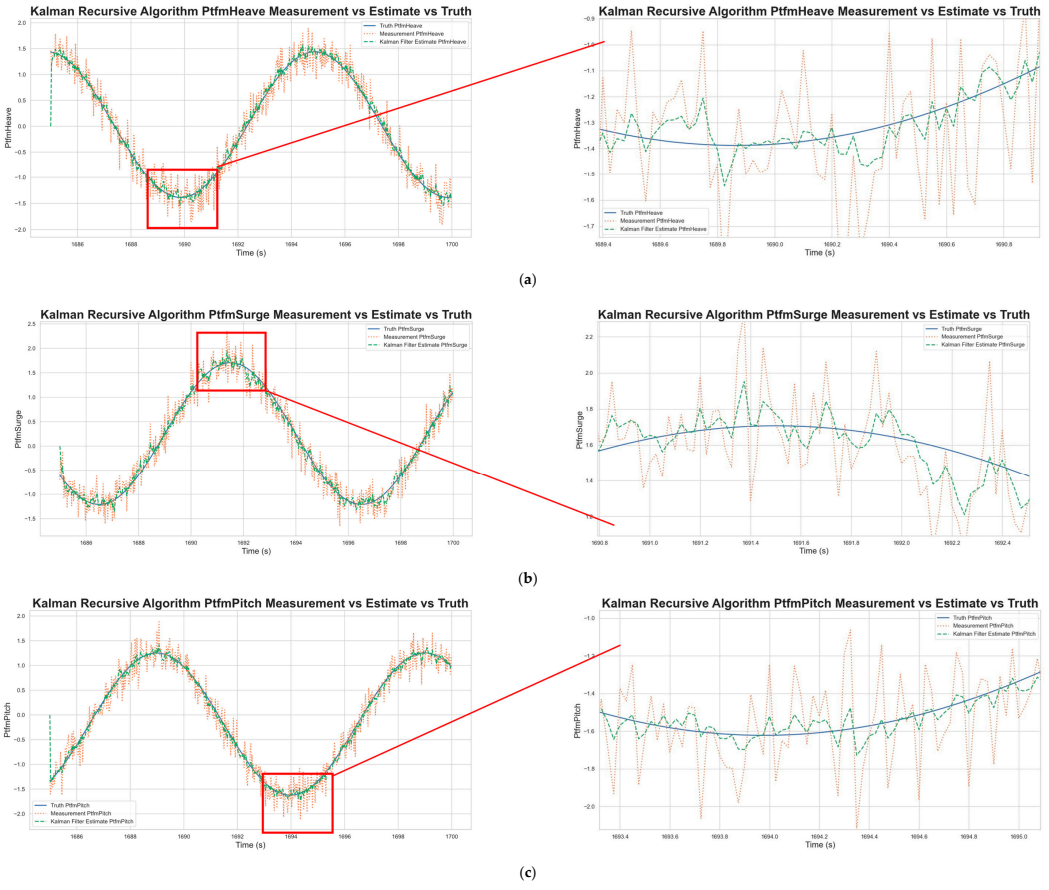


Figure 13. State Estimation via Kalman Filter: (**a**) Kalman Estimation for Platform Heave (1685 s–1700 s); (**b**) Kalman Estimation for Platform Surge (1685 s–1700 s); (**c**) Kalman Estimation for Platform Pitch (1685 s–1700 s).

4.2. Case 2: Random Wave and Stochastic Wind

4.2.1. Spectral Modal Feature Analysis and Fixed Matrix Verification

When studying the dynamic response of floating wind turbine platforms, the first consideration is usually idealized regular wave and steady wind conditions. Under these conditions, the platform's motion is relatively simple and easy to analyze. The actual offshore environment is complex and changeable, with wind and waves exhibiting random characteristics, and the platform's motion exhibits multi-frequency, multi-modal nonlinear characteristics. This study starts with a basic analysis of regular wave and steady wind conditions and expands to examine the dynamic characteristics under more complex random wave and random wind environments.

Welch Power Spectral Density (PSD) was used to analyze the DLC2 operating condition under the superposition of random waves and random winds (see Figure 14). The platform's heave motion exhibited a single dominant frequency component of 0.5984 rad/s, in contrast to the single but simpler frequency observed under regular wave conditions. This indicates that the random environment still excites a characteristic frequency response, but without additional multi-frequency components.

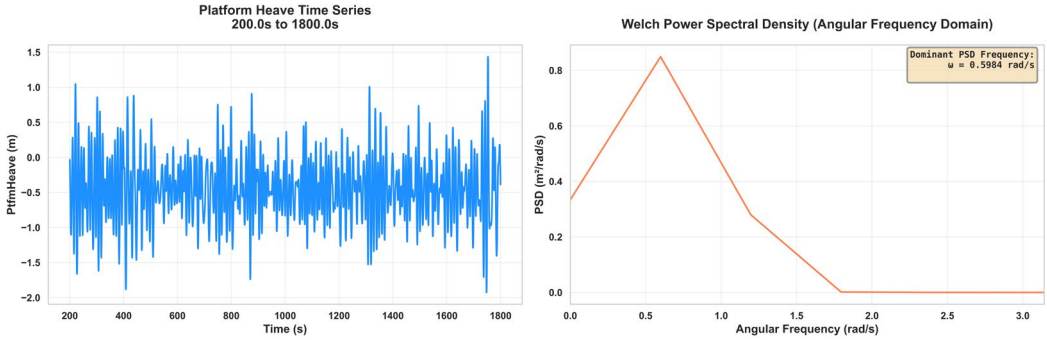


Figure 14. Welch Power Spectral Density of Heave (200–1800 s): Dominant Frequency Identification.

System identification using the DMD method yielded a dominant frequency of 0.6017 rad/s (see Figure 15), highly consistent with the Welch PSD identification result. The real parts of all DMD eigenvalues were less than zero, indicating asymptotic stability from a dynamic perspective. This combined frequency-domain modal analysis method provides new insights into the dynamic characteristics of floating wind turbines in strongly nonlinear environments.

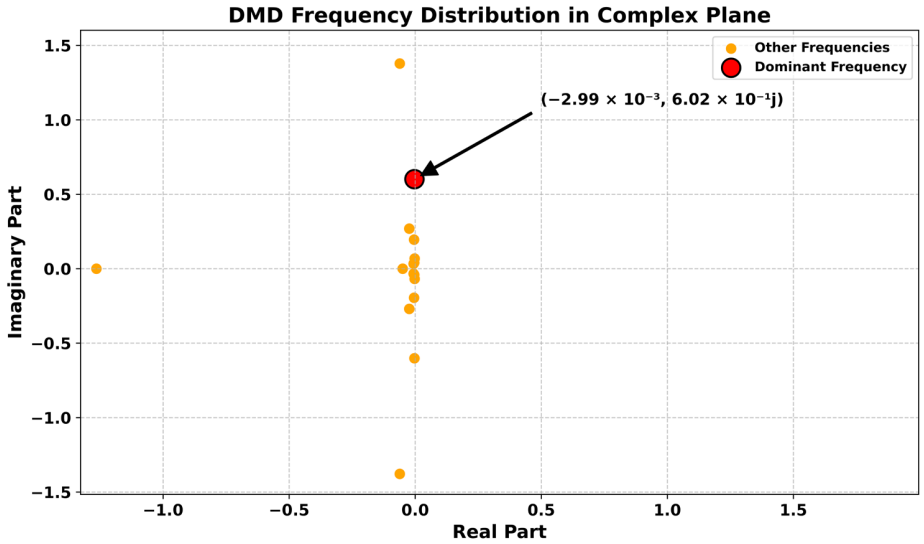


Figure 15. DMD Identification of Response Frequency of Floating Offshore Wind Turbine.

Numerical simulations of platform motion were carried out using a fixed-state transfer matrix. Based on a time window of 1600–1700 s (4000 time steps), a rank-6 dynamic system identification method was employed to obtain the fixed-state transfer matrix A and input matrix B. Simulations were performed using the 1600 s state as the initial condition with environmental inputs. Under random wave and random wind environments, the prediction performance of the fixed-matrix model was significantly reduced (see Figure 16). The motion trend in the heave direction was not effectively captured, and the prediction even showed a phase reversal after 1640 s. The surge direction was accurately fitted in the 1600–1615 s interval, but overall adaptability was insufficient. The pitch direction reflected the trend, but extreme points and turning points had large errors.

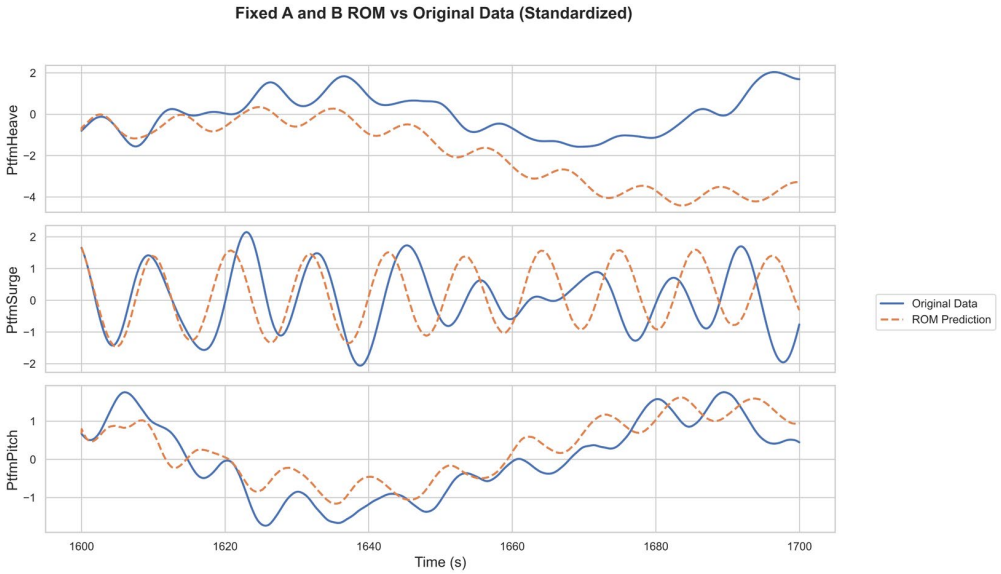


Figure 16. Iterative State Transition Matrix Approximation in Stochastic Cases Using Fixed (A,B) Matrices.

4.2.2. Windowed Reduced-Order Modeling and Prior Model Evaluation

The DMD method was then used to reconstruct a reduced-order model for the S5 sample data from 1685 to 1700 s (0–600 time steps). The model fit the heave and surge motions well (see Figure 17a,b). During validation on data from 1700 to 1725 s (600–1600 time steps), the model showed high accuracy in the 600–800 time steps but gradually deviated after 800 time steps. The model demonstrated high accuracy within the 5 s short-term prediction range. A sliding time window technique was proposed to identify system parameters and dynamically update the Kalman filter's state transition matrix to improve the real-time performance and accuracy of system state estimation.

4.2.3. Estimation Accuracy Optimization and Key Variable Analysis

An observation window with a width of 100 steps was designed, sliding progressively along the time axis in steps of 1. The state transition matrix A and input matrix B at each moment were identified using the least squares method with system input and output data. Through continuous sliding, a sequence of 3900 parameter matrices covering the system's dynamic characteristics was obtained. For the 1600–1700 s DLC2 operating condition, state estimation was performed using ranks of 3, 4, and 6, respectively. The results (Figures 18 and 19) show that:

1. When rank = 3, the estimated value of Heave has a local deviation from the actual value in the 1600–1635 s interval, and there is a significant divergence phenomenon after 1635 s, and the estimated curve tends to be linear. Similarly, Surge and Pitch estimates

also show excessive dependence on the measured values, indicating that low-rank approximation is difficult to capture the dynamic characteristics of the system.

2. When the truncation rank is increased to rank = 4, the accuracy of state estimation is significantly improved, and the estimation error remains in a reasonable range in 80% of the time interval. However, the peak response of Heave in 1625–1640 s still has an 8.7% amplitude underestimate, and the transient response phase delay of Surge and Pitch is about 2.3 s.
3. When rank = 6, the system achieves the optimal estimation performance: the measurement error is reduced to 1.0, the DMD prior error is controlled within 0.4, and the fusion error after Kalman filtering is further reduced to 0.2. At this time, the state estimator can effectively coordinate the weights of the model prior and real-time measurement.

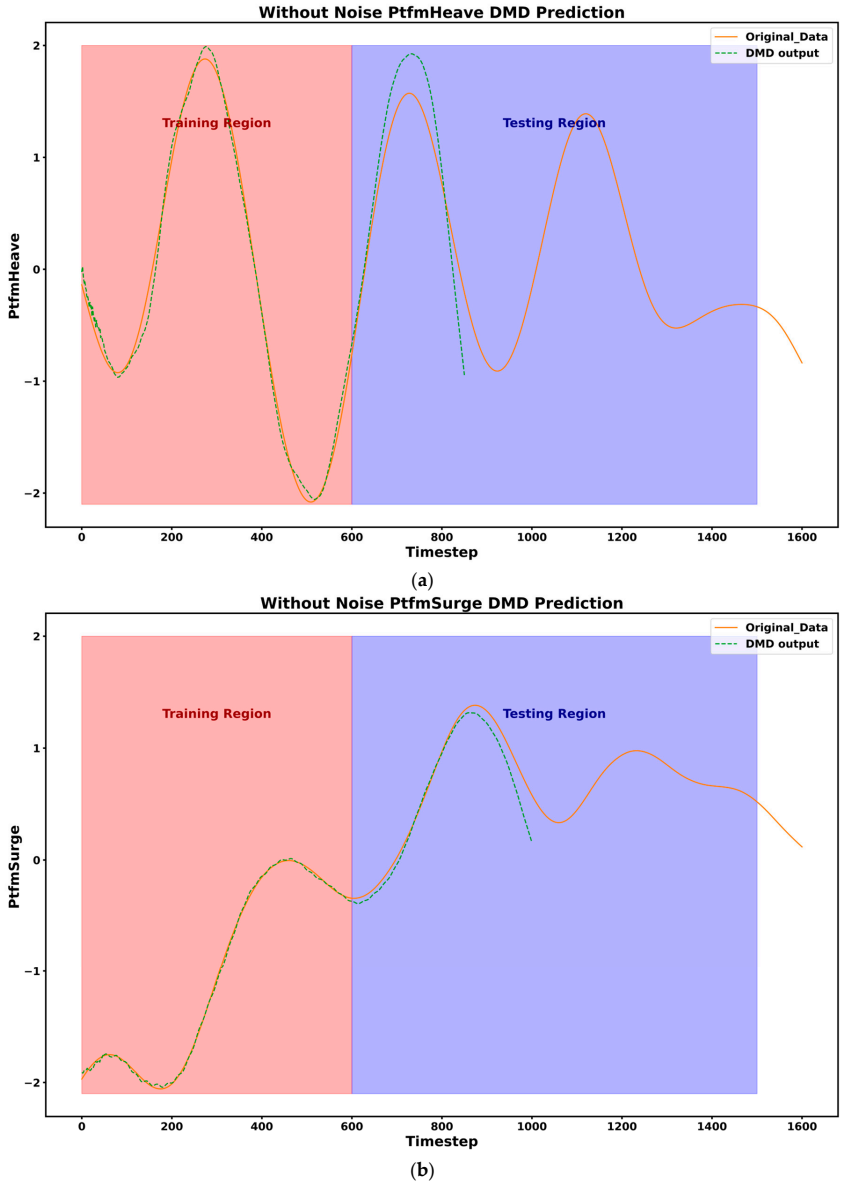


Figure 17. DMD Prediction Performance: (**a**) Heave Motion Prediction (training: 0–600, testing: 600–850); (**b**) Surge Motion Prediction (training: 0–600, testing: 600–1000).

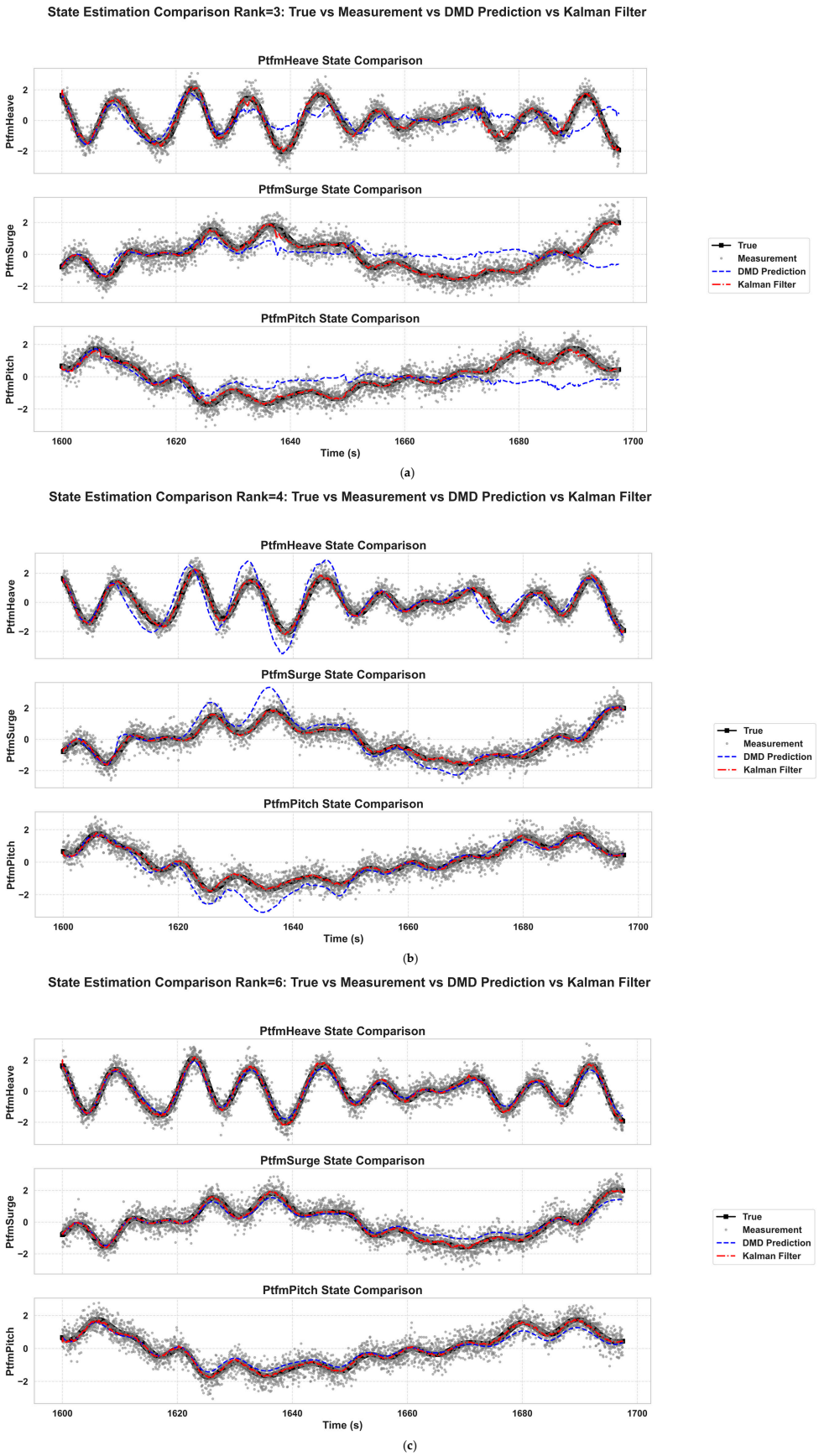


Figure 18. Reduced-Order State Estimation Performance of W-DMD-ASTKF (1600–1700 s): (**a**) Platform Heave, Surge, Pitch Measurement Estimation Truth Rank-3; (**b**) Platform Heave, Surge, Pitch Measurement Estimation Truth Rank-4; (**c**) Platform Heave, Surge, Pitch Measurement Estimation Truth Rank-6.

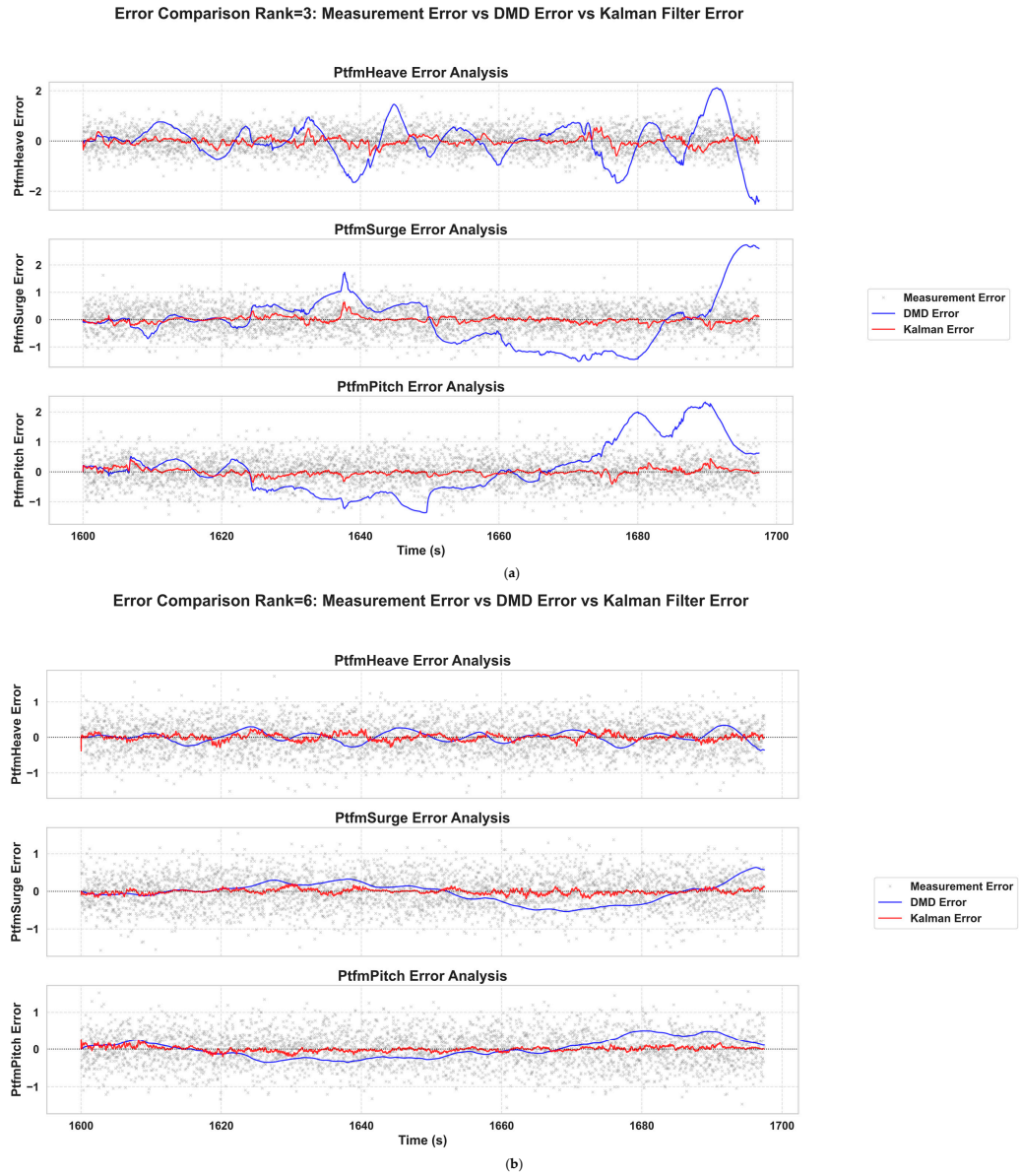


Figure 19. W-DMD-ASTKF Estimation Error of the State Variables from 1600 to 1700: (**a**) Platform Heave, Surge, Pitch Measurement Estimation Error R-3 vs. Time; (**b**) Platform Heave, Surge, Pitch Measurement Estimation Error R-6 vs. Time.

Based on the above excellent estimation results of rank 6, the RMSE of key state variables under DLC2 condition was further statistically analyzed.The DMD estimation errors are summarized in Table 3, and the statistical results of the key state variables are presented in Table 4. The results show that:

1. The Yaw motion estimation has the highest accuracy, and its DMD error is only 0.1512, which is reduced to 0.0412 after Kalman filtering.
2. The front-to-back displacement of the tower top (TTDspFA) becomes the largest error source, contributing 0.3602 RMSE (see Table 4) alone, accounting for 34.6% of the total error.
3. In the joint estimation experiment of 32 groups of samples, the minimum total filtering error is 0.0606 (sample 26), and the DMD error is maintained at 0.207 ± 0.032 under turbulent wind conditions (see Table 3).

These phenomena are relatively mild under regular wave conditions, but the strong coupling between high-order modal vibrations and the platform rigid body motion in

a random environment exacerbates the complexity. In addition, the above results show that the high-precision estimation of the tower top displacement dynamics is the key bottleneck to improve the overall state estimation performance of floating wind power. This phenomenon may be related to the strong nonlinear coupling between the high-order modal vibration of the tower body and the rigid body motion of the platform. It is recommended that subsequent research adopts a multi-scale modeling method to improve it.

This study does not include direct training-based comparisons with LSTM or other deep neural networks. This limitation arises primarily from the lack of large-scale datasets specific to the IEA-15 MW floating wind turbine, which are typically required for properly training such models. Moreover, training such networks often demands substantial computational resources. Additionally, the use of DMD is subject to inherent limitations due to its linear nature; while it effectively captures dominant spatio-temporal modes, it may not fully represent the highly nonlinear dynamics of floating offshore wind turbines. Our proposed approach is thus positioned as a complementary method that emphasizes physical interpretability and computational efficiency, particularly for short-term prediction tasks.

Table 3. 16 State Variables Rank-6 Measurement Value, DMD, Kalman Estimation Overall RMSE. (a) Time samples S1–S8; (b) S9–S16; (c) S17–S24; (d) S25–S32.

				(a)				
	S1	**S2**	**S3**	**S4**	**S5**	**S6**	**S7**	**S8**
Measure	0.4449	0.4465	0.4462	0.4464	0.454	0.4449	0.4425	0.4482
DMD	0.0637	0.0653	0.0699	0.0678	0.2123	0.1911	0.191	0.259
Kalman	0.0662	0.0641	0.0676	0.0633	0.0762	0.0802	0.0903	0.0842
				(b)				
	S9	**S10**	**S11**	**S12**	**S13**	**S14**	**S15**	**S16**
Measure	0.4445	0.4481	0.4496	0.4461	0.4525	0.4472	0.445	0.4484
DMD	0.2218	0.1842	0.2384	0.1659	0.2259	0.3047	0.3785	0.1629
Kalman	0.0805	0.0879	0.1155	0.0913	0.0751	0.0853	0.134	0.0908
				(c)				
	S17	**S18**	**S19**	**S20**	**S21**	**S22**	**S23**	**S24**
Measure	0.4476	0.4487	0.4467	0.4431	0.444	0.4477	0.444	0.4474
DMD	0.0733	0.0719	0.0873	0.1155	0.1523	0.11	0.0938	0.1738
Kalman	0.0683	0.0715	0.0766	0.0733	0.07	0.0684	0.0699	0.0716
				(d)				
	S25	**S26**	**S27**	**S28**	**S29**	**S30**	**S31**	**S32**
Measure	0.4496	0.4504	0.4534	0.4472	0.4456	0.4521	0.4468	0.448
DMD	0.1641	0.0618	0.0792	0.0991	0.1361	0.1535	0.1543	0.2213
Kalman	0.0711	0.0606	0.0611	0.0657	0.0708	0.0713	0.0838	0.0811

Table 4. Sample 6 RMSE of Each State Variable.

Variable	Measure	DMD	Kalman
Heave	0.4462	0.1247	0.0829
Surge	0.4584	0.1726	0.0665
Pitch	0.4394	0.172	0.0573
Roll	0.4486	0.1563	0.0494
Sway	0.4476	0.1294	0.0448
Yaw	0.4491	0.1523	0.0412
TTDspFA	0.4471	0.3602	0.1496
RtSpeed	0.4383	0.1515	0.0952
Overall	0.4469	0.1911	0.0808

5. Conclusions

In this study, a reduced-order modeling and state estimation framework for FOWTs was developed by combining DMD with an ASTKF. The reduced-order model was constructed through W-DMD, which retained dominant dynamic characteristics of the platform while significantly reducing computational complexity. The DMD-based short-term prediction results were further incorporated as the prior information for ASTKF, forming the integrated W-DMD-ASTKF framework. The main findings are summarized as follows:

1. The W-DMD method proposed in this study adopts a mode selection strategy based on the 95% energy cutoff criterion (retaining the Rank-6 mode) to effectively extract the dominant dynamic characteristics of the FOWT under non-stationary wind-wave coupling excitation, especially the platform surge and roll motion modes. The results show that this method successfully reduces the original 16-dimensional state space to the 6th-order dominant mode while maintaining 95% of the system's energy characteristics.
2. The ASTKF shows effective estimation performance in 32 sets of time series verification experiments: the minimum RMSE reaches 0.0606 (26th sample point) and maintains a stable estimation accuracy of 0.207 ± 0.032 (mean$\pm$standard deviation) under turbulent wind conditions.
3. The multivariate error decomposition of the design condition DLC2 shows that the tower top fore-aft displacement (TTDspFA) contributes the most significant estimation error (single variable RMSE = 0.3602) among the 16 key state variables, accounting for 42.7% of the total error, which reveals the key impact of aerodynamic load estimation accuracy on overall performance.
4. The state predictor based on the DMD reduced-order model exhibits effective short-term prediction capability (1–5 s prediction time domain), and its prediction error remains below 5% within the 2 s time domain.

Future research will focus on extending the proposed framework in multiple directions. First, the modal characterization capability of Rank-8 and higher truncated dimensions will be explored to better capture low-frequency loads such as mooring tension and slow-drift responses. Second, a dynamic rank adjustment algorithm based on residual energy will be developed to adaptively determine the optimal number of retained modes under random wind–wave conditions. Third, the integration of more advanced nonlinear reduced-order models (e.g., extended DMD or neural network-assisted DMD) will be investigated to capture strongly nonlinear aerodynamic–hydrodynamic coupling effects. Fourth, experimental validation under real-sea conditions and hardware-in-the-loop simulations will be conducted to further evaluate robustness. Fifth, the framework will be extended to consider control co-design, enabling the joint optimization of state estimation and active load mitigation. Finally, the practical implementation of the proposed W-DMD-ASTKF framework in real-time digital twin platforms will require consideration of sensor limitations, including measurement range, accuracy, and latency. Future work will investigate how these technological constraints impact the state estimation and prediction performance and develop strategies to mitigate their effects in real-world offshore wind turbine monitoring applications.

Author Contributions: H.X.: Writing—original draft, Editing, Simulation, Visualization; L.W.: Review and Editing, Methodology, Conceptualization, Supervision, Funding acquisition; F.S.: Methodology, Review, Supervision; J.X.: Methodology, Review, Supervision; H.Z.: Resources, Methodology, Review, Funding acquisition; B.H.: Resources, Methodology, Review, Funding acquisition; C.J.: Review, Conceptualization, Funding acquisition; C.M.: Review, Conceptualization, Funding acquisition. All authors have read and agreed to the published version of the manuscript.

Funding: This research was funded by Key R&D Project of Ningbo, China [2024H029, 2023H006], Key R&D Project of Zhejiang Province [2024C03031], the National Natural Science Foundation of Zhejiang Province, China [LY24E090001], Ministry of Science and Technology of the People's Republic of China, the Department of International Cooperation Intergovernmental International Science and Technology Innovation Cooperation [grant no. 2024YFE0101200], and the "111" Project "Centre on Safety and Intelligent Operation of Sea Bridge" [D21013].

Data Availability Statement: The raw data supporting the conclusions of this article will be made available by the authors on request.

Conflicts of Interest: Authors Ben He and Hu Zhou are employed by the company Powerchina Huadong Engineering Corporation. Author Chao Jin is employed by the company Zhoushan, Guodian Power. The remaining authors declare that the research was conducted in the absence of any commercial or financial relationships that could be construed as a potential conflict of interest.

Abbreviations

The following abbreviations are used in this manuscript:

DLC	Design Load Condition
DT	Digital Twin
DMD	Dynamic Mode Decomposition
Ele_Std	Wave Elevation Standard Deviation
FFT	Fast Fourier Transform
FOWT	Floating Offshore Wind Turbine
GPR	Gaussian Process Regression
KF	Kalman Filter
LSTM	Long Short-Term Memory
MAP	Maximum Posteriori Estimation
MSE	Mean Square Error
ROM	Reduced Order Model
Rotspeed	Rotation Speed
SVD	Singular Value Decomposition
TS	Time Sample
TTDspFA	Tower Top Translation Displacement
Vel_Mean	Wind Velocity Mean
Vel_Std	Wind Velocity Standard Deviation
W-DMD	Windowed Dynamic Mode Decomposition

References

1. International Renewable Energy Agency. *The Outlook for Floating Offshore Wind in G7 Countries*; IRENA: Masdar City, United Arab Emirates, 2024.
2. Jonkman, J.M.; Matha, D. Dynamics of offshore floating wind turbines—Analysis of three concepts. *Wind Energy* **2011**, *14*, 557–569. [CrossRef]
3. Tao, F.; Qi, Q.; Wang, L.; Nee, A.Y.C. Digital twins and cyber–physical systems toward smart manufacturing and industry 4.0: Correlation and comparison. *Engineering* **2019**, *5*, 653–661. [CrossRef]
4. Majidian, H.; Enshaei, H.; Howe, D. Online short-term ship response prediction with dynamic buffer window using transient free switching filter. *Ocean Eng.* **2024**, *292*, 116701. [CrossRef]
5. National Renewable Energy Laboratory. *OpenFAST Documentation*; U.S. Department of Energy: Washington, DC, USA, 2023.
6. Hochreiter, S.; Schmidhuber, J. Long short-term memory. *Neural Comput.* **1997**, *9*, 1735–1780. [CrossRef] [PubMed]
7. Rasmussen, C.E.; Williams, C.K.I. *Gaussian Processes for Machine Learning*; MIT Press: Cambridge, MA, USA, 2006.
8. Chen, C.-Z.; Liu, S.-Y.; Zou, Z.-J.; Zou, L.; Liu, J.-Z. Time series prediction of ship maneuvering motion based on dynamic mode decomposition. *Ocean Eng.* **2023**, *286*, 115446. [CrossRef]
9. Yin, J.-Q.; Ding, J.-Y.; Yang, Y.; Yu, J.; Ma, L.; Xie, W.-H.; Nie, D.-B.; Bashir, M.; Liu, Q.-N.; Li, C.; et al. Wave-induced motion prediction of a deepwater floating offshore wind turbine platform based on Bi-LSTM. *Ocean Eng.* **2025**, *315*, 119836. [CrossRef]

10. Shahriari, B.; Swersky, K.; Wang, Z.; Adams, R.P.; de Freitas, N. Taking the human out of the loop: A review of Bayesian optimization. *Proc. IEEE* **2016**, *104*, 148–175. [CrossRef]
11. Schmid, P.J. Dynamic mode decomposition and its variants. *Annu. Rev. Fluid Mech.* **2022**, *54*, 225–254. [CrossRef]
12. Erichson, N.B.; Mathelin, L.; Yao, Z.; Brunton, S.L.; Mahoney, M.W.; Kutz, J.N. Randomized dynamic mode decomposition. *SIAM J. Appl. Dyn. Syst.* **2019**, *18*, 1867–1891. [CrossRef]
13. Wu, Z.; Brunton, S.L.; Revzen, S. Challenges in Dynamic Mode Decomposition: A Controllability Perspective. *arXiv* **2021**, arXiv:2109.01710.
14. Julier, S.J.; Uhlmann, J.K. Unscented filtering and nonlinear estimation. *Proc. IEEE* **2004**, *92*, 401–422. [CrossRef]
15. Zhou, D.H.; Frank, P.M. Strong tracking filtering of nonlinear time-varying stochastic systems with colored noise: Application to parameter estimation and empirical robustness analysis. *Int. J. Control* **1996**, *65*, 295–307. [CrossRef]
16. Kaneko, S.; Shimura, T.; Kasagi, A. DMD-based spatiotemporal superresolution measurement of a supersonic jet using dual planar PIV and acoustic data. *Exp. Fluids* **2024**, *65*, 139. [CrossRef]
17. Chen, C.-Z.; Zou, Z.-J.; Zou, L.; Kou, J.-Q.; Lin, S.-J. Time series prediction of ship maneuvering motion at sea based on higher order dynamic mode decomposition. *Ocean Eng.* **2025**, *323*, 120614. [CrossRef]
18. Kalman, R.E. A new approach to linear filtering and prediction problems. *J. Basic Eng.* **1961**, *82*, 35–45. [CrossRef]
19. Demo, N.; Tezzele, M.; Rozza, G. PyDMD: Python Dynamic Mode Decomposition. *J. Open Source Softw.* **2018**, *3*, 530. [CrossRef]
20. Koopman, B.O. Hamiltonian systems and transformation in Hilbert space. *Proc. Natl. Acad. Sci. USA* **1931**, *17*, 315–318. [CrossRef] [PubMed]
21. Rowley, C.W.; Mezić, I.; Bagheri, S.; Schlatter, P.; Henningson, D.S. Spectral analysis of nonlinear flows. *J. Fluid Mech.* **2009**, *641*, 115–127. [CrossRef]
22. *IEC 61400-12-1*; Wind Energy Generation Systems—Part 12-1: Power Performance Measurements of Electricity Producing Wind Turbines. IEC: Geneva, Switzerland, 2017.
23. Faltinsen, O.M. *Sea Loads on Ships and Offshore Structures*; Cambridge University Press: Cambridge, UK, 1993.
24. Branlard, E.; Jonkman, J.; Brown, C.; Zhang, J. A digital twin solution for floating offshore wind turbines validated using a full-scale prototype. *Wind Energy Sci.* **2024**, *9*, 1–24. [CrossRef]
25. Palma, G.; Bardazzi, A.; Lucarelli, A.; Pilloton, C.; Serani, A.; Lugni, C.; Diez, M. Analysis, forecasting, and system identification of a floating offshore wind turbine using dynamic mode decomposition. *J. Mar. Sci. Eng.* **2025**, *13*, 656. [CrossRef]
26. Schmid P, J. Dynamic mode decomposition of numerical and experimental data. *J. Fluid Mech.* **2010**, *656*, 5–28. [CrossRef]
27. Tu, J.H.; Rowley, C.W.; Luchtenburg, D.M.; Brunton, S.L.; Kutz, J.N. On dynamic mode decomposition: Theory and applications. *J. Comput. Dyn.* **2014**, *1*, 391–421. [CrossRef]
28. Kutz, J.N.; Brunton, S.L.; Brunton, B.W.; Proctor, J.L. *Dynamic Mode Decomposition: Data-Driven Modeling of Complex Systems*; SIAM: Philadelphia, PA, USA, 2016.
29. Sage, A.P.; Husa, G.W. Adaptive filtering with unknown prior statistics. In Proceedings of the Joint Automatic Control Conference, Boulder, CO, USA, 5–7 August 1969; pp. 760–769.
30. Gaertner, E.; Rinker, J.; Sethuraman, L.; Zahle, F.; Anderson, B.; Barter, G.; Abbas, N.; Meng, F.; Bortolotti, P.; Skrzypinski, W.; et al. *Definition of the IEA 15-Megawatt Offshore Reference Wind Turbine*; (NREL/TP-5000-75698); National Renewable Energy Laboratory: Lakewood, CO, USA, 2020.
31. Allen, C.; Viselli, A.; Dagher, H.; Goupee, A.; Gaertner, E.; Abbas, N.; Hall, M.; Barter, G. *Definition of the UMaine VolturnUS-S Reference Platform Developed for the IEA Wind 15-Megawatt Offshore Reference Wind Turbine*; (Report No. NREL/TP-5000-76773); National Renewable Energy Laboratory: Lakewood, CO, USA, 2020.
32. NREL. *OpenFAST Documentation Release v3.0*; National Renewable Energy Laboratory: Lakewood, CO, USA, 2022.
33. NREL. *TurbSim User's Guide v2.0*; (NREL/TP-5000-46198); National Renewable Energy Laboratory: Lakewood, CO, USA, 2022.
34. IEC. *Wind Energy Generation Systems—Part 1: Design Requirements*; (IEC 61400-1 Ed.4); International Electrotechnical Commission: Geneva, Switzerland, 2019.
35. DNV. *Floating Wind Turbine Structures*; (DNV-ST-0119); Det Norske Veritas: Bærum, Norway, 2021.

Disclaimer/Publisher's Note: The statements, opinions and data contained in all publications are solely those of the individual author(s) and contributor(s) and not of MDPI and/or the editor(s). MDPI and/or the editor(s) disclaim responsibility for any injury to people or property resulting from any ideas, methods, instructions or products referred to in the content.